Available online at www.sciencedirect.com

ScienceDirect

Acta Materialia 76 (2014) 472–481

Acta MATERIALIA

www.elsevier.com/locate/actamat

Ab initio study on mechanical-bending-induced ferroelectric phase transition in ultrathin perovskite nanobelts

H.F. Li [a,b], G.H. Zhang [a,b], Yue Zheng [a,b,*], Biao Wang [a,*], W.J. Chen [a,b]

[a] *State Key Laboratory of Optoelectronic Materials and Technologies, Sun Yat-sen University, Guangzhou 510275, People's Republic of China*
[b] *Micro & Nano Physics and Mechanics Research Laboratory, School of Physics and Engineering, Sun Yat-sen University, Guangzhou 510275, People's Republic of China*

Received 30 October 2013; received in revised form 21 May 2014; accepted 27 May 2014
Available online 1 July 2014

Abstract

Based on first-principles calculations, we systematically investigated the structural, ferroelectric (FE), energetic and electronic properties of bended ultrathin $PbTiO_3$ and $BaTiO_3$ nanobelts in between flat sheet and nanotube configurations. It is found that both $PbTiO_3$ and $BaTiO_3$ ultrathin nanobelts can possess axial antiferrodistortive structural distortion (AFD distortion), and the magnitude of the AFD rotation angle is obviously determined by the bending curvature of the nanobelts. Meanwhile, spontaneous polarization can be retained in these single-unit-cell-thick nanobelts with contributions from the axial improper ferroelectricity and the radial flexoelectricity, which indicates that ultrathin perovskite nanobelts do not have a critical thickness. On the other hand, we found that the AFD distortion is stable and significant in $PbTiO_3$ nanobelts while it is metastable in $BaTiO_3$ nanobelts in comparison with the stable non-AFD structure without AFD distortion. This is due to the competition between AFD distortion and circumferential lattice extension in releasing the elastic energy in $BaTiO_3$ material. Moreover, we found that the electronic structure and bandgap of the nanobelts can be tuned by the bending curvature, indicating potential control of transport properties by mechanical bending. Our results gave more insight into the inherence of improper ferroelectricity in low-dimensional perovskite ferroelectrics.

Keywords: Ferroelectrics; Critical thickness; Improper ferroelectricity; Antiferrodistortive structural distortion; Flexoelectricity

1. Introduction

Perovskite ferroelectrics (ABO_3) are the most investigated multifunctional ferroelectrics and have a number of promising applications [1] including non-volatile ferroelectric random access memory [2]. Due to the demand for miniaturization of ferroelectric devices and the significant novelty of ferroelectricity at the nanoscale, low-dimensional perovskite ferroelectrics have attracted great interest in the field of functional materials. When the dimensions of perovskite ferroelectrics are reduced, size effects arise, including a decrease in spontaneous polarization, dielectric constant and Curie temperature as well as the reconstruction of domain structure. Due to these size effects, low-dimensional perovskite ferroelectrics often present unusual ferroelectricity, and can be used as an essential component to fabricate novel multifunctional ferroelectric nanodevices.

Among the various low-dimensional perovskite ferroelectrics, one-dimensional (1-D) ferroelectric nanostructures have not been much researched compared with

---

* Corresponding authors. Address: Micro & Nano Physics and Mechanics Research Laboratory, School of Physics and Engineering, Sun Yat-sen University, Guangzhou 510275, People's Republic of China (Y. Zheng). Tel.: +86 20 8411 3231/5692; fax: +86 8411 3231.

E-mail addresses: zhengy35@mail.sysu.edu.cn (Y. Zheng), wangbiao@mail.sysu.edu.cn (B. Wang).

http://dx.doi.org/10.1016/j.actamat.2014.05.054
1359-6454/© 2014 Acta Materialia Inc. Published by Elsevier Ltd. All rights reserved.

other nanostructures such as ultrathin films and nanoparticles. This is mainly due to the difficulty in synthesizing 1-D functional oxides. In the last decade, with the development of experimental techniques, many 1-D perovskite nanostructures have been successfully synthesized [3], such as nanowires [4–7], nanobelts [8] and nanotubes [9–12]. To date, many theoretical investigations on structures, ferroelectricity and phase transition in 1-D perovskite ferroelectrics have been performed [13–21], because there are many unknown phenomena that need to be explained and summarized.

In the research and application of low-dimensional ferroelectrics, the existence of a ferroelectric critical size is a very important issue. For a long time, it was commonly believed that there is a critical size below which the spontaneous polarization in nanoscale ferroelectrics would vanish due to effects of the surface, interface and depolarization fields [22–25]. However, a critical size does not always exist in low-dimensional ferroelectrics. For example, studies have revealed that there is no intrinsic ferroelectric critical thickness in epitaxial perovskite ultrathin films and ferroelectric tunnel junctions under certain conditions [26–30]. In recent years, the investigation of improper ferroelectricity [31] has revealed it as a new potential mechanism explaining the absence ferroelectric critical size in certain nanoscale ferroelectrics. For example, Shimada et al. [32] predicted the absence of ferroelectric thickness in $PbTiO_3$ nanotubes due to direct coupling between antiferrodistortive (AFD) rotation of TiO_6 octahedra and ferroelectric (FE) structural distortion [32]. This phenomenon (known as AFD–FE coupling improper ferroelectricity) had also been found in $PbTiO_3/SrTiO_3$ artificial superlattices by Bousquet et al. [33]. Shimada et al. [32] suggested that the presence of improper ferroelectricity in $PbTiO_3$ nanotubes results from the homogeneous compressive strain induced by the nanotubular structure. However, a coexistence of AFD and FE structural distortions on the strain-free PbO-terminated surface of bulk $PbTiO_3$ was also reported [34], which implies that the nanotubular structure is not necessary for the presence of AFD–FE coupling improper ferroelectricity.

In order to further study the AFD structural distortion and improper ferroelectricity in 1-D perovskites, we have investigated bent perovskite nanobelts. Unlike nanotubes which have a fixed and relatively large curvature, nanobelts can possess variable curvature from zero to large values, i.e. from flat sheet to nanotube configurations, and therefore the relationship between AFD distortion and bending curvature can be reflected more clearly. On the other hand, both $PbTiO_3$ and $BaTiO_3$ nanobelts have simulated investigation of the effects of ionic radii and chemical properties of different elemental species in perovskites. Our purpose is to gain more insight into the inherence of the interactions between AFD structural distortion, curvature-induced strain, ferroelectric polarization and electronic structure of 1-D perovskite ferroelectric, and explore the essence of the unusual AFD distortion and AFD–FE coupling phenomena.

2. Model and method

In following simulations, we perform density functional calculations (DFT) within the local density approximation implemented in the Vienna Ab initio Simulation Package (VASP) [35,36]. A schematic illustration of the simulated perovskite nanobelts is shown in Fig. 1a. To be convenient and clear, we adopt a cylindrical coordinate system (defined by longitudinal axis z, radial distance ρ and angular coordinate φ) with longitudinal axis parallel to the z axis of the rectangular coordinate system. The nanobelt is modeled by bending a single-unit-cell-thick 1-D ABO_3 flat sheet around an axis parallel to the z axis (the flat sheet is infinitely long in the z direction). Within the periodic boundary conditions (PBCs), to ensure the thickness of the vacuum layer between periodic images in the x–y direction is larger than 20 Å (most first-principles works have found that a 20 Å thick vacuum layer between periodic images is sufficient), we place the nanobelt in the center of a 90 Å × 90 Å × c supercell with c determined by structural relaxation. A nanobelt with its BO_2 surface compressed is defined as an up-bending nanobelt, as shown in Fig. 1b. Conversely, a nanobelt with its AO surface compressed is defined as a down-bending nanobelt, as shown in Fig. 1c. For simplicity of discussion, we further specify the curvature of up-bending nanobelts to be positive and the down-bending nanobelts to be negative. For an infinitely long nanotube, there are two surfaces (the inner and outer surfaces), while a bent nanobelt has two extra side surfaces along the φ direction (the left and right surfaces) as shown in Fig. 1b and c. These two surfaces cause a side surface effect, which tends to reduce the calculated physical quantities (AFD rotation angle, axial polarization and radial polarization) in the 2–3 unit cells adjacent to the side surfaces, as shown in Tables 1 and 2. This side effect was also demonstrated to play an important role in the polarization pattern in nanowires [37]. In our simulation, all nanobelts have a width of 16 ABO_3 unit cells in the φ direction. Meanwhile, to reflect the side surface effect, for all the calculated physical quantities, an averaging over the 16 unit cells of the nanobelt is adopted.

We use the projector-augmented wave method for the electron–ion interactions [38]. The cut-off energy of plane wave basis is set to 500 eV. We adopt a mesh of $1 \times 1 \times 3$ Monkhorst–Pack k-point for k-point sampling in the Brillouin zone [39]. As our supercell has a huge size in the x–y direction, a relatively sparse k-point mesh can help us to avoid unbearably slow self-consistent calculations. We calculate the polarizations in the z direction of highly bent nanobelts with the number of k-points in z direction increased from 1 to 3, and found that the results are close to Shimada et al.'s results in nanotubes when $k_z = 3$ [32]. Considering that the side surface effect would reduce the average polarization in a nanobelt relative to a nanotube, it seems that the $1 \times 1 \times 3$ k-point mesh slightly overestimates the axial polarization. Nevertheless, we consider that the results are still quite accurate. The structural

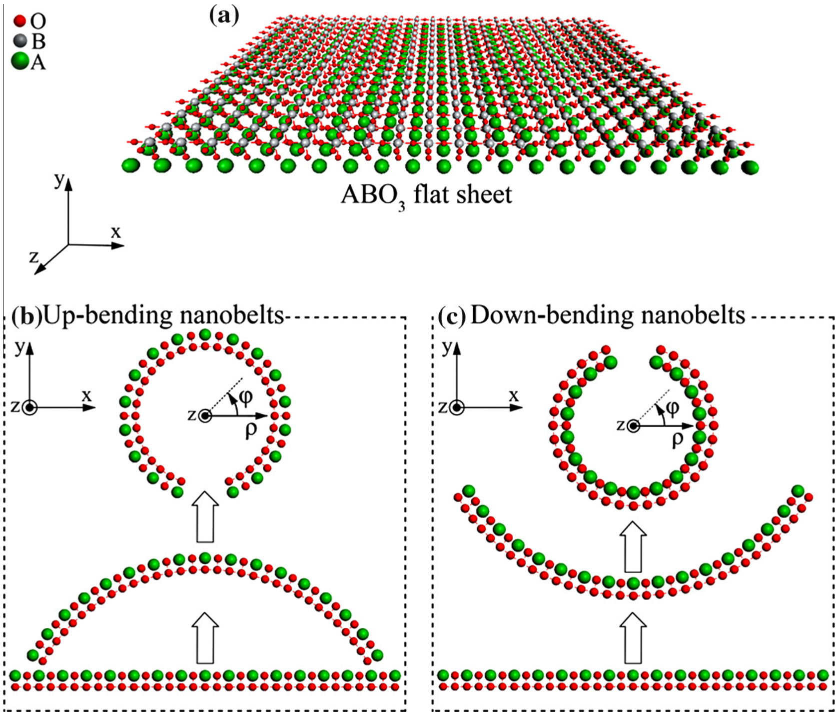

Fig. 1. Schematic illustrations of (a) ABO_3 flat sheet and the two bent configurations of (b) up-bending nanobelts and (c) down-bending nanobelts.

Table 1
The distribution of calculated AFD rotation angle, axial polarization and radial polarization in the 16 $PbTiO_3$ unit cells along the φ direction of $PbTiO_3$ nanobelts with curvatures of −0.096, 0 and 0.096 $Å^{-1}$.

$PbTiO_3$ nanobelts	AFD rotation angle (degrees)			Axial polarization ($\mu C\ cm^{-2}$)			Radial polarization ($\mu C\ cm^{-2}$)		
Curvature ($Å^{-1}$)	−0.096	0	0.096	−0.096	0	0.096	−0.096	0	0.096
Unit cell 1	0.09	9.05	14.53	0.00	1.15	4.46	−1.06	1.37	2.64
Unit cell 2	0.10	10.12	15.60	0.00	1.28	5.10	−1.64	2.07	4.02
Unit cell 3	0.11	10.63	16.11	0.00	1.35	5.36	−2.07	2.61	5.07
Unit cell 4	0.11	10.94	16.42	0.00	1.39	5.51	−2.16	2.73	5.32
Unit cell 5	0.11	11.07	16.55	0.00	1.40	5.58	−2.19	2.74	5.33
Unit cell 6	0.11	11.14	16.62	0.00	1.41	5.61	−2.20	2.76	5.35
Unit cell 7	0.11	11.17	16.63	0.00	1.41	5.63	−2.22	2.78	5.46
Unit cell 8	0.11	11.15	16.65	0.00	1.41	5.62	−2.22	2.80	5.46
Unit cell 9	0.11	11.14	16.62	0.00	1.41	5.61	−2.21	2.79	5.45
Unit cell 10	0.11	11.11	16.61	0.00	1.40	5.60	−2.22	2.80	5.44
Unit cell 11	0.11	11.08	16.56	0.00	1.40	5.58	−2.21	2.80	5.44
Unit cell 12	0.11	10.97	16.45	0.00	1.39	5.53	−2.18	2.75	5.35
Unit cell 13	0.10	10.77	16.25	0.00	1.36	5.42	−2.17	2.72	5.29
Unit cell 14	0.10	10.44	15.92	0.00	1.32	5.27	−2.05	2.56	5.03
Unit cell 15	0.10	10.01	15.49	0.00	1.27	5.04	−1.62	2.05	3.99
Unit cell 16	0.09	9.00	14.47	0.00	1.14	4.53	−1.06	1.34	2.62

relaxation is performed by fixing the x–y coordinates of the Pb/Ba atoms on the side surfaces of $PbTiO_3$/$BaTiO_3$ nanobelts and freely relaxing all other atoms, this corresponds to mechanically clamped nanobelts in experiment (i.e. using two tweezers to grip the Pb/Ba atoms on the side surfaces and then bending the nanobelt). All the bent nanobelts are fully relaxed until all the atomic force components (except for the fixed atoms) are smaller than 0.01 eV $Å^{-1}$. In order to obtain the AFD distortion in the nanobelts via structural relaxation, a tiny rotary perturbation of TiO_5 pyramids around the z axis is introduced into the initial nanobelt structure to reduce the system's symmetry. Meanwhile, for comparison, we also simulate the nanobelts without TiO_5 pyramid rotary perturbation, and therefore we get two distinct final optimized nanobelt structures: (i) the AFD structure (perturbed), in which the TiO_5 pyramids rotate to a certain degree; and (ii) the non-AFD structure (unperturbed), in which the TiO_5 pyramids do not rotate, though the atomic positions and lattice parameters are still optimized.

Table 2
The distribution of calculated AFD rotation angle, axial polarization and radial polarization in the 16 $BaTiO_3$ unit cells along the φ direction of $BaTiO_3$ nanobelts with curvatures of −0.096, 0 and 0.096 $Å^{-1}$.

$BaTiO_3$ nanobelts	AFD rotation angle (degrees)			Axial polarization ($\mu C\ cm^{-2}$)			Radial polarization ($\mu C\ cm^{-2}$)		
Curvature ($Å^{-1}$)	−0.096	0	0.096	−0.096	0	0.096	−0.096	0	0.096
Unit cell 1	0.00	0.15	9.60	0.00	0.00	0.52	−0.31	0.28	1.31
Unit cell 2	0.00	0.31	9.77	0.00	0.00	0.60	−0.52	0.40	1.93
Unit cell 3	0.00	0.46	9.92	0.00	0.00	0.62	−0.63	0.52	2.39
Unit cell 4	0.00	0.52	9.98	0.00	0.00	0.64	−0.69	0.53	2.51
Unit cell 5	0.00	0.55	10.01	0.00	0.00	0.65	−0.66	0.54	2.52
Unit cell 6	0.00	0.56	10.02	0.00	0.00	0.65	−0.67	0.54	2.53
Unit cell 7	0.00	0.56	10.02	0.00	0.00	0.65	−0.67	0.55	2.56
Unit cell 8	0.00	0.57	10.03	0.00	0.00	0.65	−0.71	0.55	2.58
Unit cell 9	0.00	0.57	10.02	0.00	0.00	0.65	−0.68	0.56	2.57
Unit cell 10	0.00	0.56	10.02	0.00	0.00	0.65	−0.70	0.54	2.59
Unit cell 11	0.00	0.56	10.02	0.00	0.00	0.65	−0.70	0.54	2.56
Unit cell 12	0.00	0.56	10.02	0.00	0.00	0.64	−0.69	0.54	2.54
Unit cell 13	0.00	0.52	9.97	0.00	0.00	0.63	−0.68	0.54	2.51
Unit cell 14	0.00	0.56	9.91	0.00	0.00	0.61	−0.66	0.51	2.39
Unit cell 15	0.00	0.30	9.76	0.00	0.00	0.59	−0.48	0.39	1.88
Unit cell 16	0.00	0.13	9.59	0.00	0.00	0.53	−0.31	0.28	1.28

3. Results and discussions

3.1. Stability analysis of AFD structural distortion in $PbTiO_3$/$BaTiO_3$ nanobelts

In order to illustrate the AFD distortion in the $PbTiO_3$ and $BaTiO_3$ nanobelts, the cross-sections of the atomic structures of AFD $PbTiO_3$ and $BaTiO_3$ nanobelts with $\kappa = 0.096\ Å^{-1}$ are shown in Fig. 2. The in-plane buckling of the TiO_2 surface induced by the periodic clockwise and counterclockwise rotations of the TiO_5 pyramids around the z axis, i.e. the AFD rotation, can be clearly observed in both $PbTiO_3$ and $BaTiO_3$ nanobelts, as was previously reported in ultrathin $PbTiO_3$ nanotubes [32].

The total energy per perovskite unit cell of both AFD and non-AFD nanobelts as a function of nanobelt curvature $\kappa = 1/R$ (where R is the average of the outer and inner surface radii of the nanobelt) is shown in Fig. 3 (the energy of the corresponding non-AFD flat sheet is set as the zero point). From Fig. 3a, it is clear that the total energies of the AFD and non-AFD structures are almost the same in the down-bending ($\kappa < 0$) $PbTiO_3$ nanobelts, while the total energy of the AFD structure dramatically decreases below the non-AFD structure in the up-bending $PbTiO_3$ nanobelts, indicating that AFD distortion plays an important role in stabilizing the atomic structure of the up-bending $PbTiO_3$ nanobelts. Meanwhile, the $BaTiO_3$ nanobelts exhibit behaviors different to those of the $PbTiO_3$ nanobelts. As shown in Fig. 3b, the total energy of non-AFD $BaTiO_3$ nanobelts is lower than that of AFD nanobelts irrespective of which direction they bend toward. Analysis of total energy indicates that the $BaTiO_3$ nanobelt tends not to undergo AFD distortion, while the $PbTiO_3$ nanobelt can undergo significant AFD distortion if a compressive strain is applied to its TiO_2 surface, i.e. bending it towards the TiO_2 surface. Another interesting result worth noting is that from Fig. 3 it can be seen that while there is a minimum in energy for the $PbTiO_3$ up-bending nanobelt, the energy for the $BaTiO_3$ nanobelt keeps decreasing as the positive curvature increases. Further calculation has been made to compare the energy of TiO_2-outside nanotubes, nanobelts with a curvature of $-0.096\ Å^{-1}$, flat sheets, nanobelts with a curvature of $0.096\ Å^{-1}$ and PbO/BaO-outside nanotubes of $PbTiO_3$ and $BaTiO_3$, as shown in Table 3. The results indicate that the one-unit-cell-thick $PbTiO_3$/$BaTiO_3$ nanotubes are more stable than the corresponding nanobelts as the two side surfaces are combined. The minimum in energy for $PbTiO_3$ up-bending nanobelts

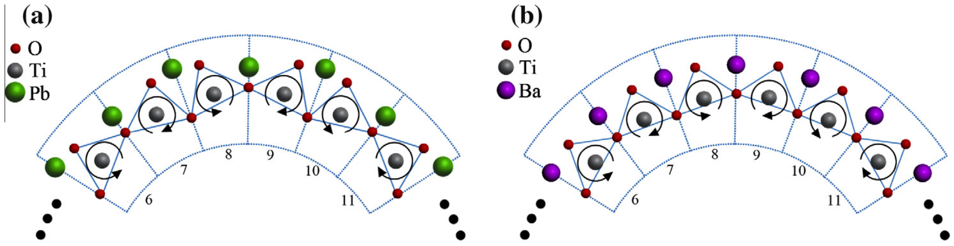

Fig. 2. Cross-sections of AFD distortion in (a) a bent $PbTiO_3$ nanobelt and (b) a bent $BaTiO_3$ nanobelt.

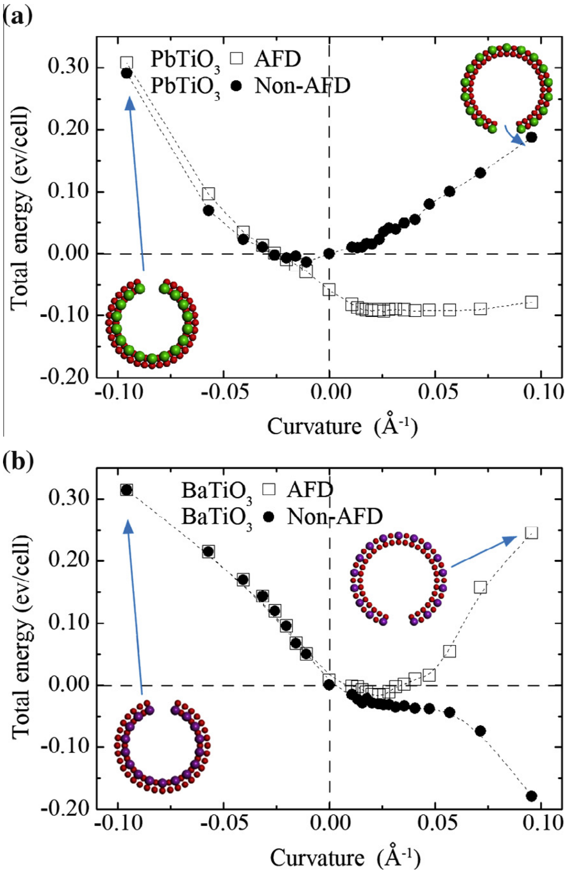

Fig. 3. Total energy per unit cell as a function of curvature in (a) $PbTiO_3$ nanobelt and (b) $BaTiO_3$ nanobelt. The total energy of the non-AFD flat sheet is set to zero.

Table 3
Calculated total energy of nanotubes, nanobelts and flat sheets.

Structures	Total energy (eV/cell)	
	$PbTiO_3$	$BaTiO_3$
Nanotube ($\kappa = -0.109$ Å^{-1})	−34.36	−35.76
Nanobelt ($\kappa = -0.096$ Å^{-1})	−35.26	−36.87
Flat sheet	−35.57	−37.18
Nanobelt ($\kappa = 0.096$ Å^{-1})	−35.63	−37.37
Nanotube ($\kappa = 0.109$ Å^{-1})	−36.44	−39.30

is most likely results from competition between bending and AFD distortion (bending would increase the energy while AFD distortion would decrease the energy), while the $BaTiO_3$ nanobelt simply tends to curl up to form a BaO-outside nanotube to minimize its energy.

We have seen that AFD distortion in $PbTiO_3$ nanobelts is energetically favorable, whereas $BaTiO_3$ nanobelts tend not to undergo AFD distortion. To obtain more insight into these behaviors, the evolutions of relaxation for AFD $PbTiO_3$ and non-AFD $BaTiO_3$ nanobelts with $\kappa = 0.096$ Å^{-1} are depicted in Fig. 5. We can see that the preferred relaxation process for $PbTiO_3$ nanobelts is a typical AFD distortion, while it is a circumferential lattice extension for the $BaTiO_3$ nanobelts. Fig. 5a shows that the presence of AFD rotation in $PbTiO_3$ nanobelts results from O ions moving toward adjacent Pb ions, which is most likely due to the strong covalent interaction between O and Pb ions. Meanwhile, recent research has revealed that the formation of short covalent Pb–O bonds is an important mechanism for the presence of the AFD distortion in $PbTiO_3$ [34]. Furthermore, it is known that strain also influences the presence of AFD distortion [32,40]. For our simulated ABO_3 nanobelts, a strong compression of the TiO_2 atomic layer will lead to the presence of layer buckling and AFD distortion while tension can weaken it or make it disappear. As a result, the AFD rotation is enhanced in up-bending $PbTiO_3$ nanobelts, while in non-AFD up-bending $PbTiO_3$ nanobelts, the AFD rotation is unstable and the total energy of the system dramatically increases (see Fig. 2a) relative to that of the AFD nanobelts. In down-bending $PbTiO_3$ nanobelts, the stretching of TiO_2 surface results in the weakening of AFD distortion as expected. However, in $BaTiO_3$ nanobelts, the interaction between Ba and O ions is weaker than that between Pb and O ions, leading to difficulty in shortening Ba–O bonds and forming AFD distortion [41,42]. The bent $BaTiO_3$ nanobelts tend to release strain energy via moving their atoms outward along the radial direction as shown in Fig. 5b, which results in a significant extension of the lattice in the circumferential direction. Although large compressive strain applied to TiO_2 surface would force $BaTiO_3$ nanobelts to undergo AFD distortion as shown in Fig. 2b, it is a metastable state as we illustrated above. It has been reported that there is a weak AFD distortion in bulk $PbTiO_3$ while the bulk $BaTiO_3$ is stable against the AFD distortion [43]. Importantly, for nanobelts, we can clearly see that the AFD distortion is significantly enhanced in the ultrathin $PbTiO_3$ nanobelts, whereas the $BaTiO_3$ nanobelts are still stable against the AFD distortion.

According to previous research [43], the stiffness of the R-point AFD phonon mode ($\kappa^R = \frac{1}{2}\partial^2 E/\partial\phi^2$, where ϕ is the AFD rotation angle) in bulk perovskite material is proportional to the Goldschmidt tolerance factor $t = (r_A + r_O)/\left[\sqrt{2}(r_B + r_O)\right]$ in many cases [44], where r_A, r_B and r_O are the radii of the A ion, B ion and O ion, respectively. The tolerance factor is a characterization of the mismatch of ionic radii in perovskite. It can be used to determine the symmetry of the ground state. We suggest that it should also be helpful in perovskite nanobelts, i.e. perovskite oxides with small A ions or large B ions such as $CaTiO_3$, $SrTiO_3$ and $PbZrO_3$ are possibly suitable materials for synthesizing nanobelts with strong AFD distortive instability, while perovskites which have larger Goldschmidt tolerance factors than $BaTiO_3$ may not be suitable for this application. On the other hand, in some perovskites there are mechanisms other than ionic radii mismatch determining the structure; these perovskites include $PbTiO_3$ (the lone pair of Pb strongly affects the structure), $LaMnO_3$ (Jahn–Teller distortion forms to lift orbital degeneracy), etc. As a result, the conclusions derived from the tolerance factor are not absolute.

3.2. The influence of nanobelt curvature on AFD structural distortion

The AFD rotation angle ϕ as a function of nanobelt curvature κ is shown in Fig. 4. Based on the total energy analysis, a red solid line connects the ϕ of the more stable structure, i.e. the AFD nanobelt or non-AFD nanobelt. That is to say, the red line labels the reasonable evolutionary path of ϕ as κ changes. It can be seen that the AFD rotation angle of the bent $PbTiO_3$ nanobelt increases with the increasing positive curvature (up-bending), whereas it decreases rapidly with the increasing negative curvature (down-bending). Large AFD distortion can be obtained in the up-bending $PbTiO_3$ nanobelt, with ϕ continuously increasing to 16° above. Moreover, significant AFD distortion ($\phi = 11.1°$) is obtained in the $PbTiO_3$ flat sheet, which is consistent with the reported existence of intrinsic AFD instability in epitaxial $PbTiO_3$ thin film [29,45]. The AFD distortion in the bent $BaTiO_3$ nanobelt exhibits a distinct behavior, as shown in Fig. 4b. The AFD distortion in the $BaTiO_3$ flat sheet and bent nanobelts with curvature <0.048 Å^{-1} is not obvious (the optimized ϕ in AFD structure is <4°). On the other hand, a relatively significant AFD distortion ($\varphi > 4°$) is obtained when κ is >0.048 Å^{-1}, which is metastable relative to the non-AFD structure (see Fig. 3b). Therefore it is easier to generate AFD distortion in $PbTiO_3$ nanobelts than in $BaTiO_3$ nanobelts.

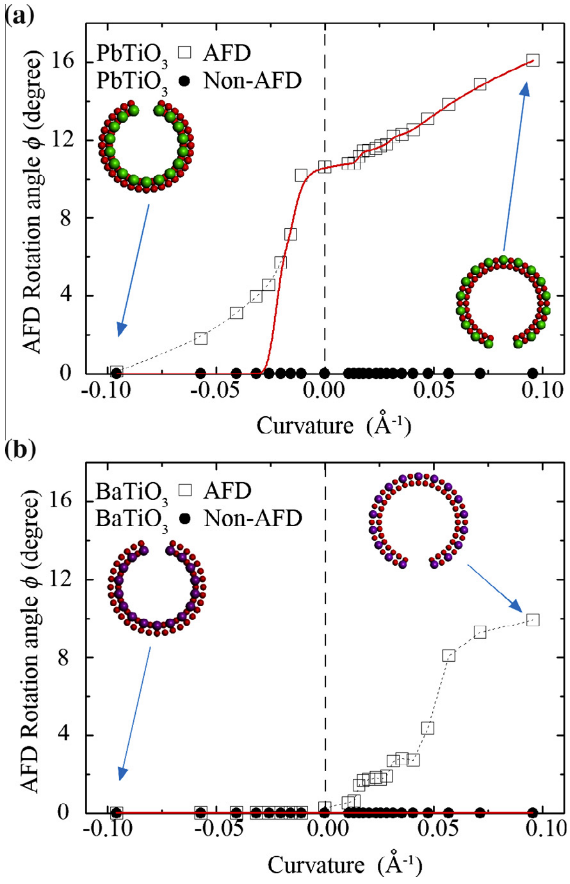

Fig. 4. AFD rotation angle ϕ as a function of nanobelt curvature in $PbTiO_3$ and $BaTiO_3$ nanobelts. The inserts depict the corresponding bending nanobelts. The positive and negative curvatures represent the up-bending and down-bending nanobelts, respectively. The red line labels the ϕ of the structure which has the lower energy, i.e. the AFD or non-AFD nanobelt.

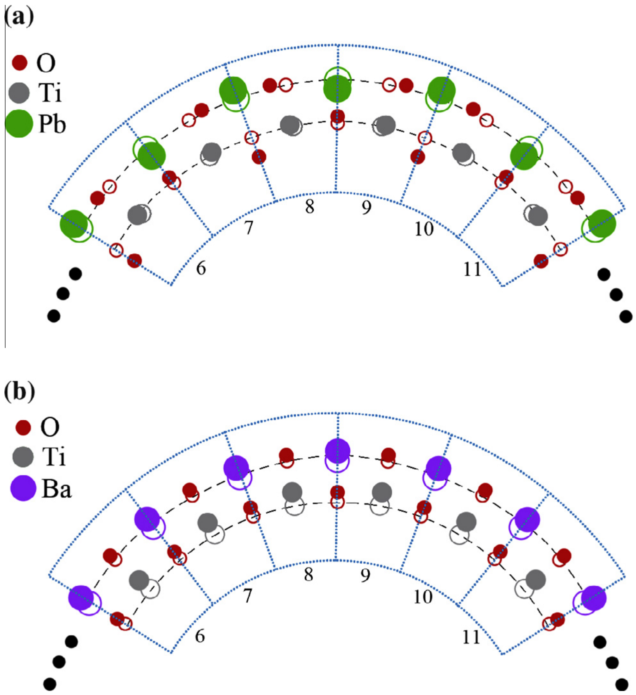

Fig. 5. Evolutions of relaxation for (a) AFD $PbTiO_3$ nanobelt with $\kappa = 0.096$ Å^{-1} and (b) non-AFD $BaTiO_3$ nanobelt with $\kappa = 0.096$ Å^{-1}. Hollow circles represent the positions of atoms in the initial structure, while solid circles represent the positions of atoms in the final optimized structure. Note that (a) is a typical AFD distortion while (b) is a circumferential lattice extension.

3.3. Spontaneous polarization in $PbTiO_3$/$BaTiO_3$ nanobelts

In the following, we investigate the ferroelectric polarization of the nanobelts. Within the cylindrical coordinate system, the total polarization of a nanobelt has three components: radial polarization (P_ρ), circumferential polarization (P_φ) and axial polarization (P_z). The polarization is calculated using $\vec{P} = (1/\Omega)\sum_\alpha Z^*_\alpha \vec{u}_\alpha$, where Ω is the volume of the ABO_3 unit cell in the nanobelt, Z^*_α is the Born effective charge calculated using density functional perturbation theory (DFPT) method [46] for the atom α in a flat sheet, and $\vec{u}_\alpha$ is the displacement vector of the atom α in relative to the paraelectric configuration. The calculated atomic Born effective charges in $PbTiO_3$ and $BaTiO_3$ flat sheets are listed in Tables 4 and 5, and the corresponding values in bulk materials are also provided. The axial polarization P_z as a function of curvature for $PbTiO_3$ and $BaTiO_3$ nanobelts is shown in Fig. 6a and b, respectively. It can be clearly seen that P_z increases as the AFD rotation angle ϕ increases in both $PbTiO_3$ and $BaTiO_3$ nanobelts due to direct AFD–FE coupling. This result is in good agreement with Ref. [32]. In addition, we found that the $PbTiO_3$

flat sheet possesses a small non-zero axial polarization, which is also initiated by AFD distortion, while bent $BaTiO_3$ nanobelts and flat sheets are always unstable with respect to axial polarization.

The radial polarization P_ρ as a function of curvature for $PbTiO_3$ and $BaTiO_3$ nanobelts is shown in Fig. 6c and d, respectively, where positive P_ρ represents a radial polarization pointing to the AO surface while negative P_ρ represents a radial polarization pointing to the BO_2 surface. It is clear that P_ρ increases as the curvature increases in up-bending $PbTiO_3$ and $BaTiO_3$ nanobelts. Meanwhile, P_ρ decreases and reverses its direction as the curvature decreases in down-bending $PbTiO_3$ and $BaTiO_3$ nanobelts. Furthermore, P_ρ of the AFD structures is larger than that of the non-AFD structures, indicating that the AFD distortion also contributes to the radial polarization. Moreover, P_ρ of the $BaTiO_3$ nanobelt is smaller than that of the $PbTiO_3$ nanobelt. Theoretically, a bent ABO_3 nanobelt would possess radial flexoelectricity [47,48]. Research into flexoelectricity is a rapidly developing field and a series of works have recently revealed its mechanism and discussed its application [49–53]. From our result, it is clear that P_ρ tends to reverse its direction as the bending direction of the nanobelts is reversed, which is consistent with the characteristic of flexoelectricity. The contribution to radial polarization from flexoelectricity can be expressed as

Table 4
Calculated atomic Born effective charges in bulk material and in a single-unit-cell-thick flat sheet of $PbTiO_3$.

$PbTiO_3$	Z^*_{Pb}	Z^*_{Ti}	$Z^*_{O_\parallel}$	$Z^*_{O_\perp}$
Unit cell 1	$\begin{bmatrix} 1.17 & 0.14 & \\ 0.06 & 0.62 & \\ & & 3.40 \end{bmatrix}$	$\begin{bmatrix} 3.25 & 0.22 & \\ 0.04 & 0.95 & \\ & & 6.77 \end{bmatrix}$	$\begin{bmatrix} -0.94 & 0.21 & \\ & -0.45 & \\ & & -6.89 \end{bmatrix}$	$\begin{bmatrix} -1.87 & 0.45 & \\ 0.04 & -0.56 & \\ & & -2.03 \end{bmatrix}$
Unit cell 2	$\begin{bmatrix} 1.81 & 0.11 & \\ 0.02 & 0.54 & \\ & & 3.76 \end{bmatrix}$	$\begin{bmatrix} 3.95 & 0.20 & \\ & 0.85 & \\ & & 7.66 \end{bmatrix}$	$\begin{bmatrix} -1.20 & 0.03 & \\ & -0.45 & \\ & & -7.49 \end{bmatrix}$	$\begin{bmatrix} -3.19 & -0.05 & \\ & -0.41 & \\ & & -2.27 \end{bmatrix}$
Unit cell 3–14	$\begin{bmatrix} 1.96 & & \\ & 0.56 & \\ & & 3.85 \end{bmatrix}$	$\begin{bmatrix} 4.00 & & \\ & 0.85 & \\ & & 7.85 \end{bmatrix}$	$\begin{bmatrix} -1.29 & & \\ & -0.45 & \\ & & -7.65 \end{bmatrix}$	$\begin{bmatrix} -3.42 & & \\ & -0.39 & \\ & & -2.31 \end{bmatrix}$
Unit cell 15	$\begin{bmatrix} 1.81 & -0.11 & \\ -0.02 & 0.54 & \\ & & 3.76 \end{bmatrix}$	$\begin{bmatrix} 3.95 & -0.20 & \\ & 0.85 & \\ & & 7.66 \end{bmatrix}$	$\begin{bmatrix} -1.20 & -0.03 & \\ & -0.45 & \\ & & -7.49 \end{bmatrix}$	$\begin{bmatrix} -3.19 & 0.05 & \\ & -0.41 & \\ & & -2.27 \end{bmatrix}$
Unit cell 16	$\begin{bmatrix} 1.17 & -0.14 & \\ -0.06 & 0.62 & \\ & & 3.40 \end{bmatrix}$	$\begin{bmatrix} 3.25 & -0.22 & \\ -0.04 & 0.95 & \\ & & 6.77 \end{bmatrix}$	$\begin{bmatrix} -0.94 & -0.21 & \\ & -0.45 & \\ & & -6.89 \end{bmatrix}$	$\begin{bmatrix} -1.87 & -0.45 & \\ -0.04 & -0.56 & \\ & & -2.03 \end{bmatrix}$
Bulk(cubic, 3.87 Å)	3.90	7.57	−6.26	−2.61

Table 5
Calculated atomic Born effective charges in bulk material and in a single-unit-cell-thick flat sheet of $BaTiO_3$.

$BaTiO_3$	Z^*_{Ba}	Z^*_{Ti}	$Z^*_{O_\parallel}$	$Z^*_{O_\perp}$
Unit cell 1	$\begin{bmatrix} 1.21 & 0.31 & \\ 0.08 & 0.81 & \\ & & 2.09 \end{bmatrix}$	$\begin{bmatrix} 3.70 & 0.44 & \\ -0.11 & 1.02 & \\ & & 7.89 \end{bmatrix}$	$\begin{bmatrix} -1.22 & -0.11 & \\ -0.05 & -0.52 & \\ & & -7.43 \end{bmatrix}$	$\begin{bmatrix} -2.11 & 0.31 & \\ 0.23 & -0.60 & \\ & & -2.29 \end{bmatrix}$
Unit cell 2	$\begin{bmatrix} 1.48 & 0.04 & \\ 0.01 & 0.65 & \\ & & 2.80 \end{bmatrix}$	$\begin{bmatrix} 4.54 & 0.09 & \\ 0.04 & 0.95 & \\ & & 8.61 \end{bmatrix}$	$\begin{bmatrix} -1.40 & -0.02 & \\ -0.02 & -0.48 & \\ & & -8.11 \end{bmatrix}$	$\begin{bmatrix} -3.44 & -0.01 & \\ & -0.42 & \\ & & -2.38 \end{bmatrix}$
Unit cell 3–14	$\begin{bmatrix} 1.61 & & \\ & 0.68 & \\ & & 2.85 \end{bmatrix}$	$\begin{bmatrix} 4.53 & & \\ & 0.95 & \\ & & 8.84 \end{bmatrix}$	$\begin{bmatrix} -1.38 & & \\ & -0.48 & \\ & & -8.23 \end{bmatrix}$	$\begin{bmatrix} -3.66 & & \\ & -0.40 & \\ & & -2.43 \end{bmatrix}$
Unit cell 15	$\begin{bmatrix} 1.48 & -0.04 & \\ -0.01 & 0.65 & \\ & & 2.80 \end{bmatrix}$	$\begin{bmatrix} 4.54 & -0.09 & \\ -0.04 & 0.95 & \\ & & 8.61 \end{bmatrix}$	$\begin{bmatrix} -1.40 & 0.02 & \\ 0.02 & -0.48 & \\ & & -8.11 \end{bmatrix}$	$\begin{bmatrix} -3.44 & 0.01 & \\ & -0.42 & \\ & & -2.38 \end{bmatrix}$
Unit cell 16	$\begin{bmatrix} 1.21 & -0.31 & \\ -0.08 & 0.81 & \\ & & 2.09 \end{bmatrix}$	$\begin{bmatrix} 3.70 & -0.44 & \\ 0.11 & 1.02 & \\ & & 7.89 \end{bmatrix}$	$\begin{bmatrix} -1.22 & 0.11 & \\ 0.05 & -0.52 & \\ & & -7.43 \end{bmatrix}$	$\begin{bmatrix} -2.11 & -0.31 & \\ -0.23 & -0.60 & \\ & & -2.29 \end{bmatrix}$
Bulk (cubic, 3.94 Å)	2.75	7.79	-6.15	-2.18

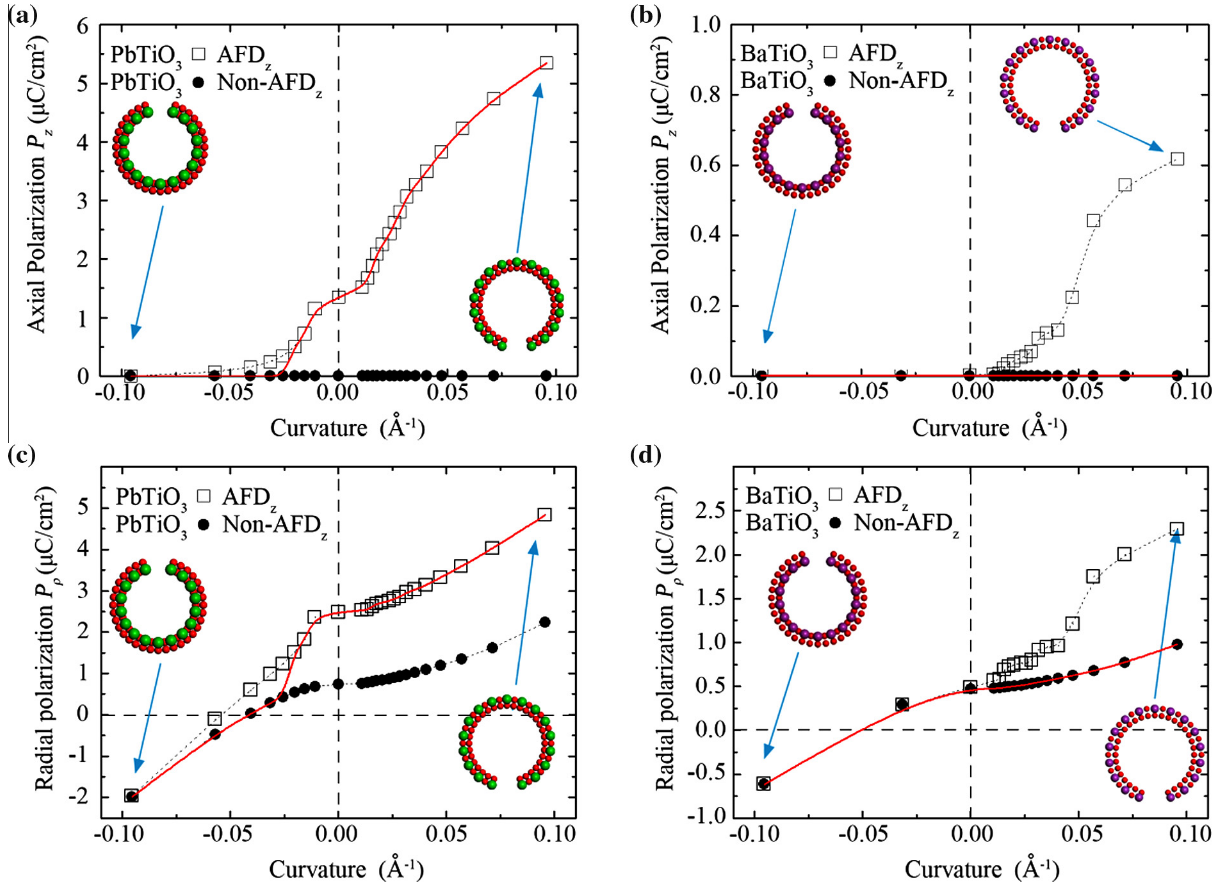

Fig. 6. Axial polarization P_z as a function of nanobelt curvature in (a) $PbTiO_3$ and (b) $BaTiO_3$ nanobelts, and the radial polarization P_ρ as functions of nanobelt curvature in (c) $PbTiO_3$ and (d) $BaTiO_3$ nanobelts. The red line marks the P_z or P_ρ of the nanobelt which has the lower total energy between the AFD and non-AFD nanobelts. (For interpretation of the references to color in this figure legend, the reader is referred to the web version of this article.)

$P_\rho^{flexo} = \mu^*(\partial\varepsilon_{11}/\partial\rho)$, where μ^* is the effective flexoelectric coefficient which is a combination of longitudinal coefficient and transverse coefficient, and $\partial\varepsilon_{11}/\partial\rho$ is the transverse strain gradient along the radial direction. Interestingly, we found non-zero spontaneous polarizations perpendicular to the surface in both $PbTiO_3$ and $BaTiO_3$ flat sheets (2.5 μC cm^{-2} for $PbTiO_3$ flat sheet and 0.5 μC cm^{-2} for $BaTiO_3$ flat sheet). Both polarizations are an order of magnitude smaller than that of calculated bulk values (78.1 μC cm^{-2} for $PbTiO_3$ and 32.0 μC cm^{-2} for $BaTiO_3$). Under normal circumstances, an ultrathin flat sheet is unlikely to possess an out-of-plane polarization due to the strong depolarization field. However, as our calculated flat sheets have asymmetric surfaces, which result in the presence of a built-in electric field, a small spontaneous radial polarization can be expected. Such polarization perpendicular to surface was also found to be stable in ferroelectric nanowires [37]. On the other hand, we found that the circumferential polarization P_φ is negligible, in contrast with the circumferential polarization in nanotubes predicted in Ref. [32]. This is likely due to our calculated nanobelts being free from axial stress and strain, while an axial compressive strain is needed to trigger circumferential polarization in nanotubes. The circumferential ferroelectricity obtained in $PbTiO_3$ nanotubes by Shimada et al. is most likely a reflection of the circumferential piezoelectricity, as the axial compressive strain will result in the presence of circumferential stretching strain.

In addition to the AFD–FE coupling and flexoelectricity, there is an interesting possibility of coupling between AFD rotation and strain gradient, which could be termed flexo-antiferroelectricity. Since the nanobelts we simulated are one unit cell thick, we cannot study the changes in the oxygen octahedra rotation angle along the strain gradient direction (i.e. the radial direction), but we expect that this phenomenon will be very obvious in a thicker nanobelt. As for the existence of AFD–FE coupling, the flexo-antiferroelectricity could tune the electronic polarization, and thus is a new kind of interaction between strain gradient and polarization that differs from flexoelectricity. We hope that more works can be implemented and provide more in-depth discussions on this interesting subject.

3.4. Electronic properties of $PbTiO_3$/$BaTiO_3$ nanobelts

Finally, we have calculated the electronic properties of $PbTiO_3$ and $BaTiO_3$ nanobelts. The cross-sections of an

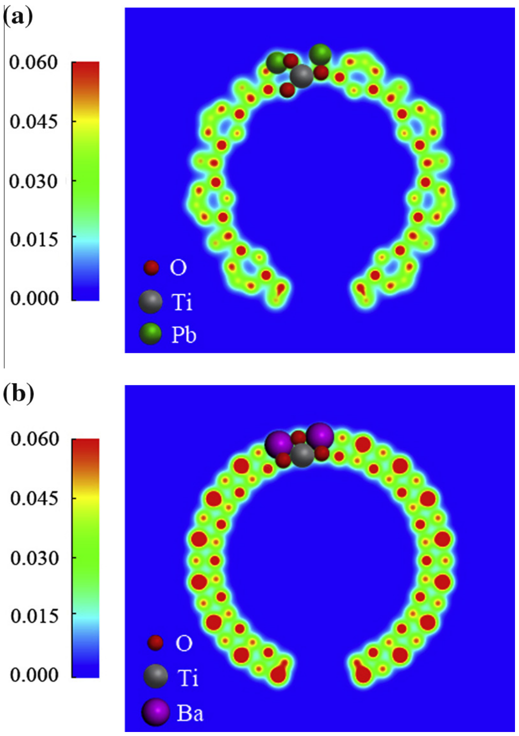

Fig. 7. Cross-sections of charge density contour profile in (a) AFD $PbTiO_3$ nanobelt with $\kappa = 0.096$ Å^{-1} and (b) non-AFD $BaTiO_3$ nanobelt with $\kappa = 0.096$ Å^{-1}.

AFD $PbTiO_3$ nanobelt with $\kappa = 0.096$ Å^{-1} and a non-AFD $BaTiO_3$ nanobelt with $\kappa = 0.096$ Å^{-1} are shown in Fig. 7. From the picture we can clearly see the different ionic radii of Pb and Ba ions as well as the different chemical bonding situations in $PbTiO_3$ and $BaTiO_3$ nanobelts. The density of states (DOS) of bulk materials, nanobelts and flat sheets are shown in Fig. 8. Considering the underestimation of band gap within the framework of the LDA approximation and the relatively sparse k-point mesh we used, the LDA+U method is employed to improve the description of ground state electron gas. Following the recommended values provided in CASTEP, the on-site d-orbital effective Hubbard U is set to 2.5 eV for Ti atoms and 2 eV for Nb atoms. The insulating property of the calculated materials is found to be properly described under these parameters. As shown in Fig. 8, the bulk materials have the smallest calculated band gap compared with low-dimensional structures ($E_g^{PbTiO_3}$(bulk) = 1.70 eV and $E_g^{BaTiO_3}$(bulk) = 1.68 eV). The band gap is also sensitive to any change in bending curvature. Specifically, with curvature ranging from −0.096 to 0.096 Å^{-1}, the $PbTiO_3$ nanobelt band gap increases from 2.71 to 3.52 eV, and the $BaTiO_3$ nanobelt band gap of increases from 1.84 to 3.25 eV. These results suggest that ultrathin nanobelts may possess stronger resistance to electric current leakage than bulk materials, and the transport properties can be tuned by altering the nanobelt curvature.

4. Summary and conclusions

We have systematically investigated the structural, ferroelectric and energetic properties of bent ultrathin $PbTiO_3$ and $BaTiO_3$ nanobelts based on first-principles calculations. It is found that both $PbTiO_3$ and $BaTiO_3$ nanobelts can possess axial AFD distortion, which will result in an axial polarization. With contributions from the axial ferroelectricity triggered by the AFD distortion and the radial flexoelectricity, spontaneous polarization can be retained in these single-unit-cell-thick nanobelts, which indicates that these materials do not have a critical thickness. Moreover, we find that the AFD distortion in $PbTiO_3$ nanobelts

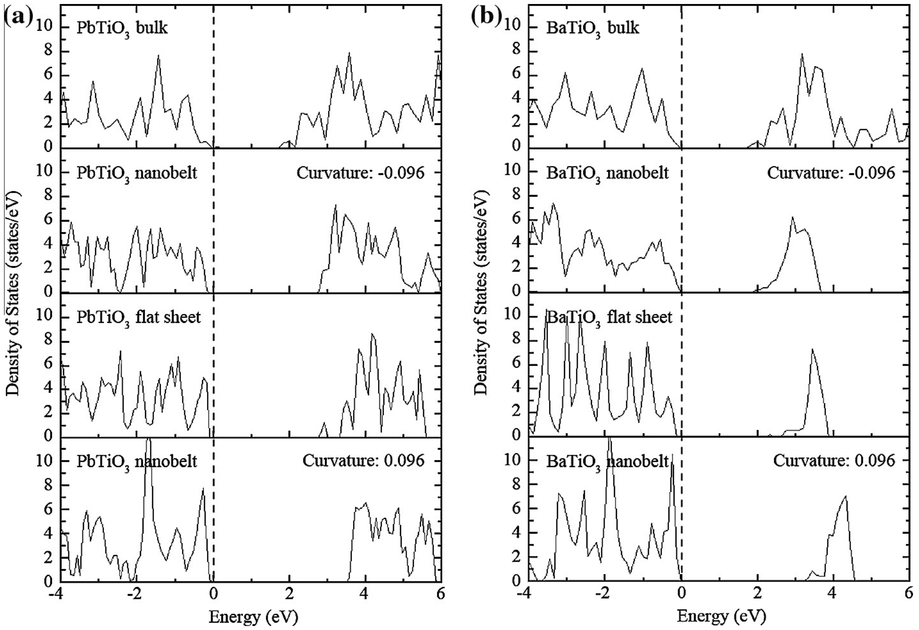

Fig. 8. Calculated density of states (DOS) of bulk material, flat sheet and nanobelt of (a) $PbTiO_3$ and (b) $BaTiO_3$. The corresponding valence band maximum (VBM) is set as the zero point of energy.

is stable and significant. In contrast, the non-AFD structure is stable in $BaTiO_3$ nanobelts where the AFD distortion is metastable. An up-bending $PbTiO_3$ nanobelt tends to undergo AFD distortion due to the compressive strain applied to its TiO_2 interface and the strong interaction between Pb and O atoms. In contrast, due to the difficulty in shortening the Ba–O bond, a $BaTiO_3$ nanobelt prefers to release flexural strain energy via the circumferential lattice extension rather than by AFD reconstruction. Moreover, the electronic structure and band gap of the nanobelts can be tuned by adjusting the bending curvature, which implies that the potential electroresistance effect can be controlled by mechanical bending. Our calculations provide insightful results and discussions on improper ferroelectricity in ultrathin perovskite nanobelts and are expected to be verified by future theoretical and experimental investigations.

Acknowledgements

The authors acknowledge the financial support of the National Natural Science Foundation of China (NSFC) (Nos. 10902128, 10732100, 50802026, and 10972239). Y.Z. is also grateful for support from the Fundamental Research Funds for the Central Universities, New Century Excellent Talents in University, Research Fund for the Doctoral Program of Higher Education, Fok Ying Tung Foundation, Guangdong Natural Science Funds for Distinguished Young Scholar.

References

[1] Bhalla AS, Guo R, Roy R. Mater Res Innovations 2000;4:3.
[2] Ishiwara H. J Nanosci Nanotechnol 2012;12:7619.
[3] Rorvik PM, Grande T, Einarsrud MA. Adv Mater 2011;23:4007.
[4] Limmer SJ, Seraji S, Forbess MJ, Wu Y, Chou TP, Nguyen C, et al. Adv Mater 2011;13:1269.
[5] Mao YB, Banerjee S, Wang SS. J Am Chem Soc 2003;125:15718.
[6] Wang W, Ke H, Rao JC, Feng M, Zhou Y. J Alloy Compd 2010;504:367.
[7] Murphy CJ, Jana NR. Adv Mater 2002;14:80.
[8] Wu J, Xue DF. Nanoscale Res Lett 2011;6:14.
[9] Mao YB, Banerjee S, Wang SS. Chem Commun 2003;2003:408.
[10] Yang Y, Wang XH, Sun CK, Li LT. J Appl Phys 2011;109:014109.
[11] Xin YC, Jiang J, Huo K, Hu T, Chu PK. ACS Nano 2009;3:3228.
[12] Yan CL, Nikolova L, Dadvand A, Harnagea C, Sarkissian A, Perepichka DF, et al. Adv Mater 2010;22:1741.
[13] Pilania G, Ramprasad R. Phys Rev B 2010;82:155442.
[14] Shimada T, Tomoda S, Kitamura T. Phys Rev B 2009;79:024102.
[15] Zhang Y, Hong J, Liu B, Fang DN. Nanotechnology 2009;20:405703.
[16] Stachiotti MG, Sepliarsky M. Phys Rev Lett 2011;106:137601.
[17] Chen WJ, Zheng Y, Wang B. Sci Rep 2012;2:796.
[18] Slutsker J, Artemev A, Roytburd A. Phys Rev Lett 2008;100:087602.
[19] Fu H, Bellaiche L. Phys Rev Lett 2003;91:257601.
[20] Louis L, Gemeiner P, Ponomareva I, Bellaiche L, Geneste G, Ma W, et al. Nano Lett 2010;10:1177.
[21] Morozovska AN, Eliseev EA, Svechnikov GS, Kalinin SV. J Appl Phys 2010;108:042009.
[22] Junquera J, Ghosez P. Nature (London) 2003;422:506.
[23] Zheng Y, Cai MQ, Woo CH. Acta Mater 2010;58:3050.
[24] Zheng Y, Woo CH, Wang B. Nano Lett 2008;8:3131.
[25] Cai MQ, Zheng Y, Wang B, Yang GW. Appl Phys Lett 2009;95:232901.
[26] Cai MQ, Zheng Y, Ma PW, Woo CH. J Appl Phys 2011;109:024103.
[27] Pertsev NA, Kohlstedt H. Phys Rev Lett 2007;98:257603.
[28] Luo X, Wang B, Zheng Y. ACS Nano 2011;5:1649.
[29] Fong DD, Stephenson GB, Streiffer SK, Eastman JA, Auciello O, Fuoss PH, et al. Science 2004;304:1650.
[30] Aguado-Puente P, Junquera J. Phys Rev Lett 2008;100:177601.
[31] Levanyuk AP, Sannikov DG. Sov Phys Usp 1974;112:561.
[32] Shimada T, Wang XY, Kondo Y, Kitamura T. Phys Rev Lett 2012;108:067601.
[33] Bousquet E, Dawber M, Stucki N, Lichtensteiger C, Hermet P, Gariglio S, et al. Nature 2008;452:732.
[34] Bungaro C, Rabe KM. Phys Rev B 2005;71:035420.
[35] Kresse G, Furthmuller J. Phys Rev B 1996;54:11169.
[36] Kresse G, Furthmuller J. Comput Mater Sci 1996;6:15.
[37] Hong J, Catalan G, Fang DN, Artacho E, Scott JF. Phys Rev B 2010;81:172101.
[38] Kresse G, Joubert D. Phys Rev B 1999;59:1758.
[39] Monkhorst HJ, Pack JD. Phys Rev B 1976;13:5188.
[40] Janolin PE, Bouvier P, Kreisel J, Thomas PA, Kornev IA, Bellaiche L, et al. Phys Rev Lett 2008;101:237601.
[41] Kuroiwa Y, Aoyagi S, Sawada A. Phys Rev Lett 2001;87:217601.
[42] Bellaiche L, Padilla J, Vanderbilt D. Phys Rev B 1999;59:1834.
[43] Zhong W, Vanderbilt D. Phys Rev Lett 1995;74:2587.
[44] Zubko P, Gariglio S, Gabay M, Ghosez P, Triscone JM. Annu Rev Condens Matter Phys 2011;2:141.
[45] Munkholm A, Streiffer SK, Murthy MVR, Eastman JA, Thompson C, Auciello O, et al. Phys Rev Lett 2001;88:016101.
[46] Gajdos M, Hummer K, Kresse G, Furthmuller J, Bechstedt F. Phys Rev B 2006;73:045112.
[47] Tagantsev AK. Phys Rev B 1986;34:5883.
[48] Tagantsev AK. Phase Transitions 1991;35:119.
[49] Hong J, Catalan G, Scott JF, Artacho E. J Phys Condens Matter 2010;22:112201.
[50] Cross LE. J Mater Sci 2006;41:53.
[51] Hong J, Vanderbilt D. Phys Rev B 2011;84:180101(R).
[52] Lu H, Bark CW, Ojos DE, Alcala J, Eom CB, Catalan G, et al. Science 2012;336:59.
[53] Hong J, Vanderbilt D. Phys Rev B 2013;88:174107.